https://doi.org/10.5194/acp-2022-292
Preprint. Discussion started: 17 May 2022

Atmospheric Chemistry and Physics Discussions

Seasonal characteristics of atmospheric formaldehyde (HCHO) in a coastal city of southeast China: Formation mechanism and photochemical effects

Taotao Liu[1,2,3], Yiling Lin[1,4], Jinsheng Chen[1,2]*, Gaojie Chen[1,2,3], Chen Yang[1,2,3], Lingling Xu[1,2], Mengren Li[1,2], Xiaolong Fan[1,2], Yanting Chen[1,2], Liqian Yin[1,2], Yuping Chen[1,2,3], Xiaoting Ji[1,2,3], Ziyi Lin[1,2,3], Fuwang Zhang[5], Hong Wang[6], Youwei Hong[1,2]*

[1]Center for Excellence in Regional Atmospheric Environment, Institute of Urban Environment, Chinese Academy of Sciences, Xiamen, China
[2]Key Lab of Urban Environment and Health, Institute of Urban Environment, Chinese Academy of Sciences, Xiamen, China
[3]University of Chinese Academy of Sciences, Beijing, China
[4]College of Chemical Engineering, Huaqiao University, Xiamen, China
[5]Environmental Monitoring Center of Fujian, Fuzhou, China
[6] Fujian Key Laboratory of Severe Weather, Fujian Meteorological Science Institute, Fuzhou, China
Corresponding authors E-mail: Jinsheng Chen (jschen@iue.ac.cn); Youwei Hong (ywhong@iue.ac.cn)

Abstract:

Formaldehyde (HCHO) is a vital reactive carbonyl compound, which plays a critical role in the atmospheric oxidation capacity (AOC), radical chemistry, and O_3 formation. Yet, the majority of the current studies on HCHO photochemical mechanism in coastal areas remain scarce, thus limiting the full understanding of potential atmospheric impacts with limited influence from marine sources. Here, field campaigns were conducted at a typical urban site in southeast China to reveal the characteristics and potential source of ambient HCHO, as well as its impact on photochemistry, during spring and autumn of 2021. The result showed that the HCHO mixing ratios were 2.94±1.28 ppbv and 3.19±1.41 ppbv in spring and autumn, respectively. Secondary formation made the largest contributions to HCHO (49% in spring and 46% in autumn), followed by vehicle exhaust (25% and 20%) and biogenic emission (18% and 24%) in this study. Furthermore, in order to identity the impact of HCHO on photochemistry process, the formation pathways and key precursors (alkenes and aromatics) of secondary HCHO were furtherly investigated based on Observation-Based Model (OBM). The net HCHO production rate in autumn (−0.40±0.70 ppbv h^{-1}) was lower than that in spring (0.10±0.37 ppbv h^{-1}), due to the increase in HCHO loss rate under the intense solar radiation and relatively low precursor levels to limited HCHO secondary formation. Disabling HCHO mechanism decreased the abundance of OH (25% in spring and 16% in autumn), HO_2 (45%, 40%), and RO_2 (26%, 19%). Meanwhile, the net O_3 production rates dropped by 32% in spring and 29% in autumn, which were mainly dominated by the reduction of radical propagation efficiencies. The analysis of HCHO potential sources, formation pathways, and impacts on O_3 formation provided significant insights into photochemical mechanisms and pollution control in coastal areas.

Keywords: HCHO; Sources apportionment; Formation mechanism; Atmospheric oxidation capacity; Radical chemistry

https://doi.org/10.5194/acp-2022-292
Preprint. Discussion started: 17 May 2022


Atmospheric Chemistry and Physics Discussions

1 Introduction

Formaldehyde (HCHO) is an important pollutant of photochemistry, and also is one of the most abundant reactive carbonyl compounds in the troposphere, which plays a critical role in the atmospheric oxidation capacity and radical chemistry (Blas et al., 2019; Edwards et al., 2014; Bao et al., 2022). Current studies had found that the production rate of HCHO to hydroxyl radical (OH) and hydroperoxyl radical (HO_2) was 1 order of magnitude higher than that of ozone (O_3) (Zhang et al., 2021a; Liu et al., 2022a, 2022b). HCHO is also the major precursor of O_3 and secondary organic aerosols (Zeng et al., 2019; Possanzini et al., 2002; Liu et al., 2022b). Due to its sensitization, irritation, and mutagenicity, the World Health Organization (WHO) listed HCHO as a dangerous carcinogen (WHO, 2000). In recent years, HCHO has become a research focus because of its important effects on atmospheric chemistry and human health (Zeng et al., 2019).

HCHO is directly emitted from anthropogenic activities (such as vehicle exhausts and industrial activities) and natural emissions (such as biomass burning, vegetation, and sea water) (Luecken et al., 2018; Anderson et al., 2017; Lowe and Schmidt, 1983; Wittrock et al., 2006). Secondary formation of HCHO from the photo-oxidation of volatile organic compounds (VOCs) is also a significant source (Anderson et al., 2017, Zeng et al., 2019). The chemical reactions of VOCs with OH/NO_3/O_3 can produce HCHO, in which the alkoxy radical reactions (RO+O_2) have significant contributions to HCHO formation (Yang et al., 2020; Ling et al., 2017). The photolysis and oxidation with OH radicals are the main loss pathways of HCHO, which can directly produce HO_2 radicals and indirectly produce OH radicals by oxidizing NO to NO_2 (Zhang et al., 2021a; Liu et al., 2015). The OH radical is the principal oxidant for atmospheric oxidation capacity (AOC), and efficient ROx recycling (i.e. OH→RO_2→RO→HO_2→OH, ROx=OH+HO_2+RO_2) can produce O_3 (Zhang et al., 2021b). Totally, HCHO can modulate O_3 formation and AOC levels by radical chemistry, but the influencing mechanisms of HCHO on photochemistry are still complex and unclear, which helps to provide scientific guidance for further control of air pollution.

With the aggravation of O_3 pollution, the researches of HCHO have been widely reported around the world because of its significant impact on O_3 formation (Li et al., 2014; He et al., 2020; Villanueva et al., 2021; Nussbaumer et al., 2021). However, few studies on systematic field measurement of HCHO were reported in coastal cities with relatively clean atmospheric environment. In China, the relevant studies and observations were mainly focused on the megacities and regions with rapid economic development, such as Beijing, the Yangtze River Delta (YRD), and the Pearl River Delta (PRD) region. These studies about HCHO mainly focused on the pollution characteristics, sources, and identification of the dominant precursors. The major HCHO source is the methane (CH_4) oxidation in both regional background/remote PRD regions and suburban

https://doi.org/10.5194/acp-2022-292
Preprint. Discussion started: 17 May 2022

Atmospheric Chemistry and Physics Discussions

YRD regions, while isoprene (C_5H_8) was an important precursor of HCHO in a rural PRD region (Yang et al., 2021; Yang et al., 2020; Li et al., 2014). For some studies in urban sites of Beijing and the YRD region, alkenes degradation contributed most to HCHO formation (Ling et al., 2017; Liu et al., 2015). Few studies assessed that the HCHO photochemical reactions accounted for 9%–14% of atmospheric oxidation and 15% of HO_2 formation, and reducing HCHO led to a decrease of 31% in O_3 formation (Zhang et al, 2021a; Zeng et al, 2019). Currently, the researches on the influence of HCHO on atmospheric oxidation and photochemistry are still scarce. Different types and sources for HCHO precursors lead to complicated secondary formation mechanisms in various regions, thus the exploration of HCHO sources and photochemical effects are very necessary for ozone pollution mitigation by efficient control strategies.

Xiamen, a coastal city of Southeast China with relatively low atmospheric particles, frequently appeared O_3 pollution events in spring and autumn, when the meteorological conditions were governed by weather systems such as the quasi-stationary front and the west pacific subtropical high (Liu et al., 2022a; Wu et al., 2019). The favorable photochemical reaction conditions (including high air temperature, low relative humidity, intense solar radiation, and stagnant atmosphere) provided is a good 'laboratory' to further explore HCHO formation mechanism and its impact on O_3 formation. In this study, the methods of the Observation-Based Model with the Master Chemical Mechanism (OBM-MCM) and Positive Matrix Factorization (PMF) model were employed to better understand the distribution and photochemical behavior of HCHO. Our study aims to reveal (1) the seasonal characteristics and source apportionment of HCHO, (2) the HCHO formation mechanism and sensitivity to precursors, and (3) the impacts of HCHO on atmospheric oxidation capacity (AOC), radical chemistry, and O_3 formation.

2. Methodology

2.1 Site descriptions and field measurement

Xiamen is a typical southeastern coastal city located on the west coast of the Taiwan Strait. Figure 1 showed the location of the observation site (Liu et al., 2022a, 2022b). The observations of multi-parameters were based on the Atmospheric Environment Observation Supersite (AEOS, 24.61° N, 118.06° E), which was about 70 m above the ground in the Institute of Urban Environment, Chinese Academy of Sciences in Xiamen. The site is a typical urban site, surrounded by highways, shopping malls, educational institutions, administrative, and residential areas. The field campaigns were continuously conducted from May 15 to June 9, 2021, and September 5 to 30, 2021, when the typical photochemical pollution occurred frequently under the influence of various weather systems.

https://doi.org/10.5194/acp-2022-292
Preprint. Discussion started: 17 May 2022

Atmospheric Chemistry and Physics Discussions

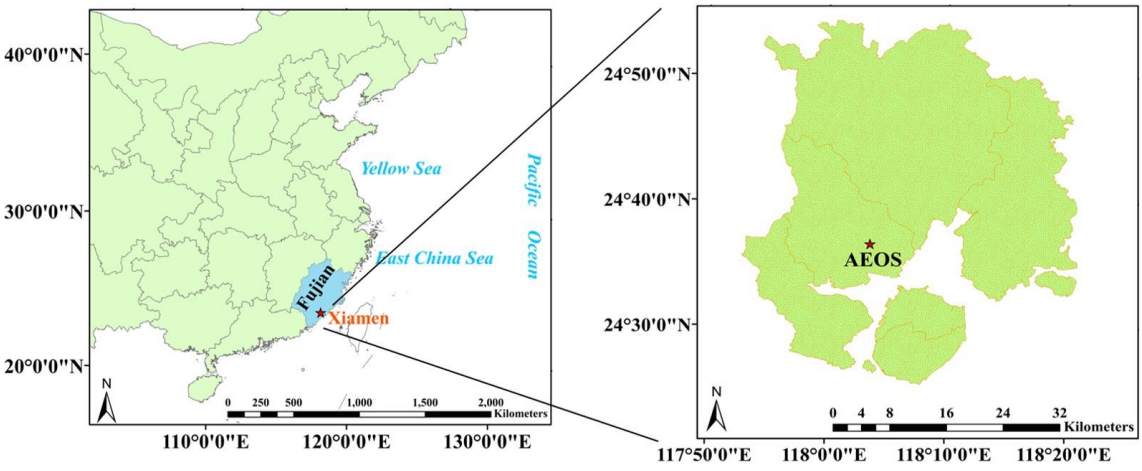

Figure 1. Location of Xiamen and the observation site.

HCHO analyzer (FMS-100, Focused Photonics Inc., Hangzhou, China) was used to monitor the HCHO mixing ratios with a temporal resolution of 1 s, which collected gaseous HCHO by an H_2SO_4 stripping solution and quantified HCHO mixing ratios through detection by fluorescence. The dilutions of the HCHO standard solution were used to make a multi-point calibration every week for obtaining a curve with R^2 ≥0.99. The limit of detection was 50 pptv and the uncertainty was ≤5% in this study. A gas chromatography coupled with a mass spectrometer (GC-FID/MS, TH-300B, Wuhan Tianhong Instruments Co., China) analyzed the VOCs with a 1-hour time resolution. The flame ionization detector (FID) using a PLOT (Al_2O_3/KCl) column (15 m × 0.32 mm × 6.0 μm) measured the hydrocarbons with 2~5 carbons; a DB-624 column (60 m × 0.25 mm × 1.4 μm) was used to quantify the other VOCs compounds. The instrument system can quantitatively analyze 106 VOCs in the ambient atmosphere, including 29 alkanes, 11 alkenes, one alkyne, 17 aromatics, 35 halogenated hydrocarbons, and 13 OVOCs (Table S1). The single-point calibration and multi-point calibration were performed every day and every month with the standard mixtures of PAMS and TO15, respectively. The detection limits of the VOCs ranged from 0.02 to 0.30 ppbv, and the precision was ≤10%.

PAN analyzer (PANs-1000, Focused Photonics Inc., Hangzhou, China) through gas chromatography with electron capture detector (GC-ECD) analyzed PAN, and the single-point calibration and the multi-point calibration were conducted every week and every month, respectively. The precision and accuracy of PAN measurements were 3% and ±10%, respectively. HONO was monitored by the Monitoring Aerosols and Gases in Ambient Air (MARGA, ADI 2080, Applikon Analytical B.V., the Netherlands), the uncertainty of which was ±10%. Criteria air pollutants (i.e. O_3, NOx, and CO) were measured by the Thermo Instruments TEI 49i, 42i, and 48i (Thermo Fisher Scientific, Waltham, MA, USA), respectively. The meteorological parameters,

https://doi.org/10.5194/acp-2022-292
Preprint. Discussion started: 17 May 2022


Atmospheric Chemistry and Physics Discussions

such as pressure (P), air temperature (T), relative humidity (RH), wind speed (WS), and wind direction (WD), were offered by a weather station with sonic anemometer (150WX, Airmar, USA). Photolysis frequencies (i.e. JHCHO, JO^1D, JNO_2, JHONO, JH_2O_2, and JNO_3) were monitored by a photolysis spectrometer (PFS-100, Focused Photonics Inc., Hangzhou, China). Table S2 shows the detailed uncertainty, detection limit, and time resolution of instruments for trace gas observation. Strict quality control and quality assurance were applied to ensure the data validity in our study, and the detailed introductions of the monitoring procedure were discussed in our previous studies (Hu et al., 2022; Liu et al., 2022a, 2020b).

2.2 Positive Matrix Factorization (PMF) model

A Positive Matrix Factorization model (PMF 5.0) was used to identify the sources of HCHO. The model decomposes a speculated sample matrix into factor contributions and profiles, as shown in Equation 1 (Norris et al., 2014):

$$e_{ij} = x_{ij} - \sum_{k=1}^{p} g_{ik} f_{kj} \quad (1)$$

where *eij* represents the residual matrix for *j* species in i sample, *xij* is the measured concentration matrix of *j* species in *i* sample, *gik* is the factor contribution matrix of *k* source in *i* sample, and *fkj* is the factor fraction matrix of *j* species in *k* source. The *Q*(*E*), the model criteria, could evaluate the stability of the solution and be calculated as follows (Sarkar et al., 2017):

$$Q(E) = \sum_{i=1}^{n} \sum_{j=1}^{m} \left(\frac{e_{ij}}{s_{ij}}\right)^2 \quad (2)$$

where s_{ij} is the standard deviation of *j* species in i sample, n and m represent the number of samples and species, respectively. The species inputting to PMF model were mainly treated as important tracers of the pollution sources. The species uncertainties need put into the model and were calculated as Equation 3, where *EF* is the error factor of 10%, and MDL is the minimum detection limit.

$$u_{ij} = \sqrt{(EF \times conc.)^2 + (MDL)^2} \quad (3)$$

In this study, 4-6 factors were tested, and all runs converged. We selected the lowest Qrobust in each run of PMF for further examination. The scaled residual needs to be between -3 and 3 for most data points. The sensitivity of the model parameters was tested with different "Extra modeling uncertainty". Q values decreased significantly with increasing uncertainty, and a value of 5% was finally chosen. We compared the lowest value of $Q_{robust}/Q_{expected}$ as the number of factors increased at each step (Brown et al., 2015). Table S3 shows that $Q_{robust}/Q_{expected}$ decreased from 4 factors to 6 factors (0.62). Displacement of factor elements (DISP) had no swaps for all factors, indicating that the solution was valid. The bootstrap (BS) of the results with 6 factors showed 80% mapping for one factor. For 4 factors, one factor for BS had 75% mapping. However, 5 factors

https://doi.org/10.5194/acp-2022-292
Preprint. Discussion started: 17 May 2022


Atmospheric Chemistry and Physics Discussions

had more than 90% mapping, and ultimately 5 factors were the optimal solution.

2.3 Observation-Based Model

As one of the important methods for analyzing atmospheric chemical processes, the Observation-Based Model (OBM) has broad application potential in deeply exploring atmospheric observation data and comprehensively understanding the regional atmospheric pollution (Zhang et al., 2021b). About the chemical mechanism, the OBM incorporating the latest chemical mechanism version of MCM-v3.3.1 (OBM-MCM, http://mcm.leeds.ac.uk/MCM/, last access: 13 May 2022) was applied to simulate the detailed photochemical processes and quantify the reaction rates of HCHO mechanism, and the OBM-MCM model introduced 142 VOCs and about 20000 chemical reactions (Jenkin et al., 2003; Saunders et al., 2003). The physical process of dry deposition and atmospheric dilution within the boundary layer height (varied from 300 m to 1500 m) was considered in the model (Li et al., 2018; Liu et al., 2022a, 2022b). Therefore, the dry deposition velocity of some atmospheric reactants showed in Table S4, which avoided continuous accumulation of pollutant concentrations in the model (Zhang et al., 2003; Xue et al., 2016).

The observed trace gases (i.e., O_3, NO, NO_2, CO, SO_2, VOCs including HCHO, PAN, and HONO), photolysis rate constants ($JHCHO$, JO^1D, JNO_2, JH_2O_2, $JHONO$, and JNO_3), and meteorological parameters (i.e., RH, T, and P) with a time resolution of 1 h were put into the OBM-MCM model, which were updated at 1 h intervals in the OBM-MCM model to constraint and localize the model. The other photolysis rates (such as OVOCs photolysis rates) were parameterized by the measured $J(NO_2)$ and the solar zenith angle (Saunders et al., 2003). Before running the model, the model was pre-run for 2 days to constrain the unmeasured species (e.g., OH, HO_2, and RO_2 radicals) reaching a steady state (Liu et al., 2022b).

The HCHO can affect O_3 formation and atmospheric oxidation capacity by radical chemistry (Yang et al., 2020; Li et al., 2014), hence the formation and loss of HCHO were discussed in our study. Furthermore, the HCHO sensitivities to their precursors were analyzed by relative incremental reactivity (RIR) (Eq. 4) (Chen et al., 2020). P(HCHO) means the net production rate of HCHO, which was calculated by the differences between HCHO production rate and loss rate (Chen et al., 2014). The ΔX/X represents the reduction ratio of each targeted HCHO precursor group, and the value adopted is 20% (Liu et al., 2022a, 2022b).

$$\mathrm{RIR(HCHO)} = \frac{\Delta \mathrm{P(HCHO)/P(HCHO)}}{\Delta \mathrm{X/X}} \qquad (4)$$

https://doi.org/10.5194/acp-2022-292
Preprint. Discussion started: 17 May 2022


Atmospheric Chemistry and Physics Discussions

3. Results and discussion

3.1 Overview of observations

The occurrence of ambient HCHO, air pollutants, and meteorological parameters were shown in Fig. 2, and the related statistical information was summarized in Table S5. The average levels of the measured HCHO in spring and autumn were 2.92±0.27 ppbv and 3.16±1.41 ppbv, respectively. The average HCHO level throughout the observation campaign (3.07±1.35 ppbv) in Xiamen was lower than that in megacities, such as Guangzhou (summer: 6.94±3.36 ppbv) (Ling et al., 2017), Shenzhen (summer: 5.00±4.40 ppbv) (Wang et al., 2017), and Beijing (summer: 11.17±5.32 ppbv) (Yang et al., 2018), but were comparable to various coastal cities with relatively clean air, including Fuzhou (Spring: 2.54±2.09 ppbv) (He et al., 2020), Shantou (autumn: 4.12±1.02 ppbv) (Shen et al., 2021), and Hong Kong (spring: 3.36±0.75 ppbv) (Lui et al., 2017), indicating the influence of anthropogenic activities and photooxidation capacity.

The average mixing ratios of HCHO in autumn were 1.08 times higher than those in spring, which was consistent with previous findings in South China (Lui et al., 2017; Wang et al., 2017). There was a relatively favorable photochemical reaction condition in autumn compared with those in spring. The O_3 mixing ratios in autumn (36.25±22.36 ppbv) were 1.23 times higher than that in spring (29.52±15.97 ppbv). Correlation analysis among HCHO, air pollutants, and meteorological parameters was shown in Table S6. As a typical secondary photochemical product, O_3 had significantly positive correlations with air temperature (0.40 in spring and 0.52 in autumn) and *J*HCHO (0.49 in spring and 0.61 in autumn), indicating that meteorological conditions obviously influenced photochemical reactions in autumn. Also, the correlation between TVOCs and HCHO in autumn (0.54) was more remarkable than that in spring (0.44). Previous studies found that high values of HCHO were mainly caused by the strong photo-oxidation of VOCs (Wolfe et al, 2016). In this study, the mixing ratios of isoprene were higher in autumn (0.41±0.54 ppbv) than that in spring (0.33±0.38 ppbv), and isoprene had a significant correlation with HCHO of 0.33 in spring and 0.64 in autumn. Correlation analysis showed O_3 and PAN had non-negligible relationships with HCHO in both seasons, and the scatter plots of HCHO along with O_3 and PAN were shown in Fig. S1. High correlations of these secondary products represented the dominance of local photochemistry during the observation period.

https://doi.org/10.5194/acp-2022-292
Preprint. Discussion started: 17 May 2022

Atmospheric Chemistry and Physics Discussions

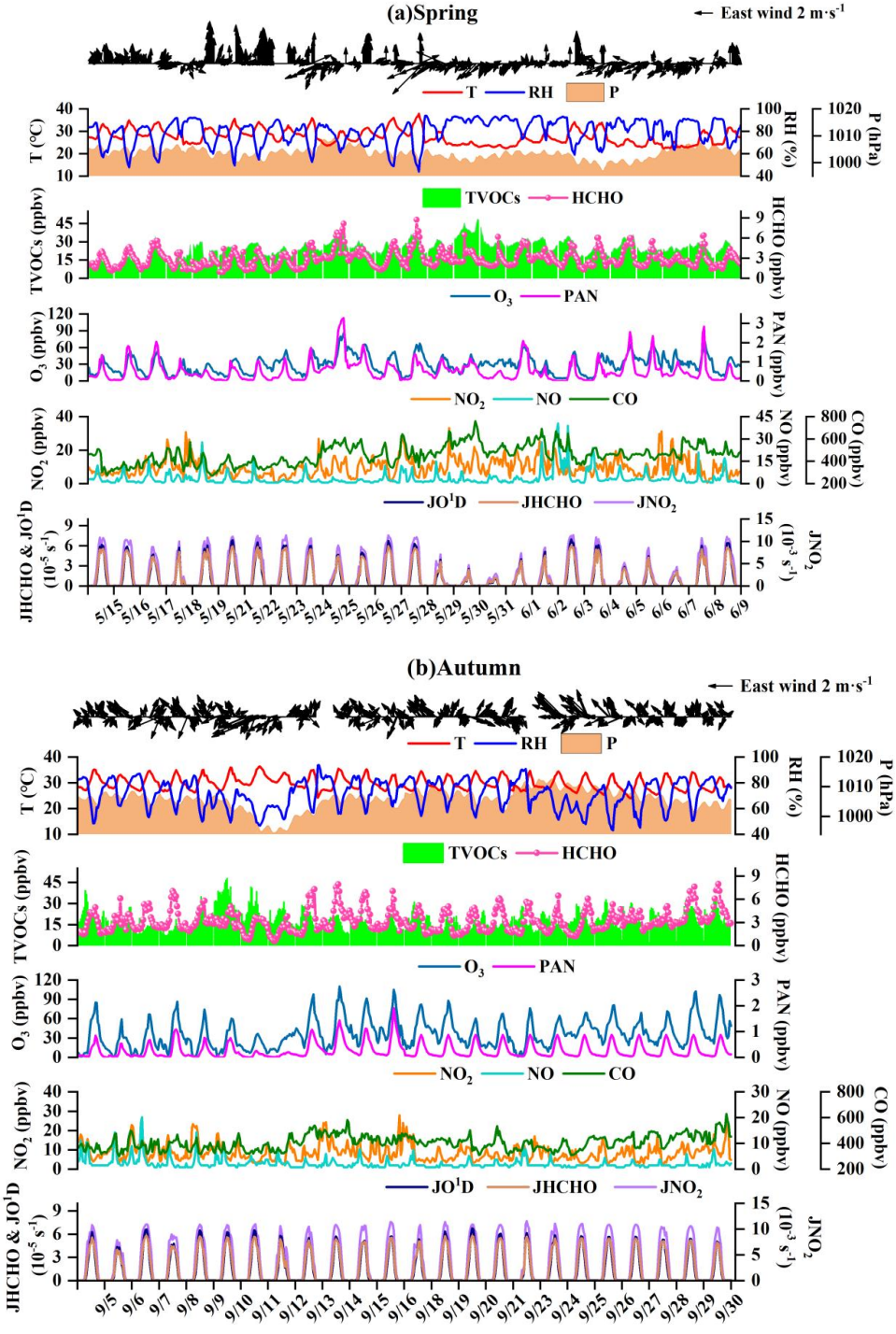

Figure 2. Time series of HCHO, air pollutants, and meteorological parameters photolysis rate constants in (a) spring and (b) autumn.

https://doi.org/10.5194/acp-2022-292
Preprint. Discussion started: 17 May 2022


Atmospheric Chemistry and Physics Discussions

As shown in Fig. 3, the diurnal variations of HCHO presented an increasing trend after sunrise at 06:00 LT (local time), peaked in the afternoon (13:00 LT), and then gradually decreased after sunset. Although the measured HCHO exhibited similar single peak variations in both seasons, the HCHO mixing ratios kept a relatively high level during the nighttime (2.34 ppbv in spring and 2.45 ppbv in autumn) compared with those during the daytime (3.49 ppbv in spring and 3.93 ppbv in autumn), which were attributed to the replenishment of HCHO primary emissions and accumulation of pollutants under stable weather conditions during the nighttime. Low wind speed at night (1.13 $m \cdot s^{-1}$ in spring and 1.73 $m \cdot s^{-1}$ in autumn) was favorable for the accumulation of air pollutants. HCHO concentration (2.09 ppbv in spring, 2.20 ppbv in autumn) was relatively low at nighttime (0:00 LT-5:00 LT), due to the influence of background contributions. While the relatively high concentration of HCHO (2.59 ppbv in spring, 2.68 ppbv in autumn) was accumulated between 18:00 LT to 23:00 LT, related to the influence of the primary HCHO emissions (e.g. vehicle exhausts) and the variety of boundary layer height. In contrast, HCHO has a short lifetime of several hours due to the quick decomposition through photolysis and reaction with OH radicals during the daytime (Lowe and Schmidt, 1983; Zhou et al., 2007). Similar diurnal patterns of HCHO, PAN, and O_3 verified the significant effects of local photochemical formation (Wang et al., 2017; Blas et al., 2019), which was consistent with the findings in previous studies (Lui et al., 2017; Ling et al., 2017; Zhang et al., 2021; Yang et al., 2018). Diurnal variations of NOx and CO, important indicators of vehicle emissions, showed a peak around 08:00 LT during the rush hours, and then increase to high values after decreasing to a minimum at 14:00-16:00 LT, which should be attributed to the impacts of photochemical depletion reaction and the height alteration of the planetary boundary layer. In addition, meteorological parameters (T, RH, JHCHO, and JO^1D) in autumn have a significant difference from those in spring.

https://doi.org/10.5194/acp-2022-292
Preprint. Discussion started: 17 May 2022

Atmospheric Chemistry and Physics Discussions

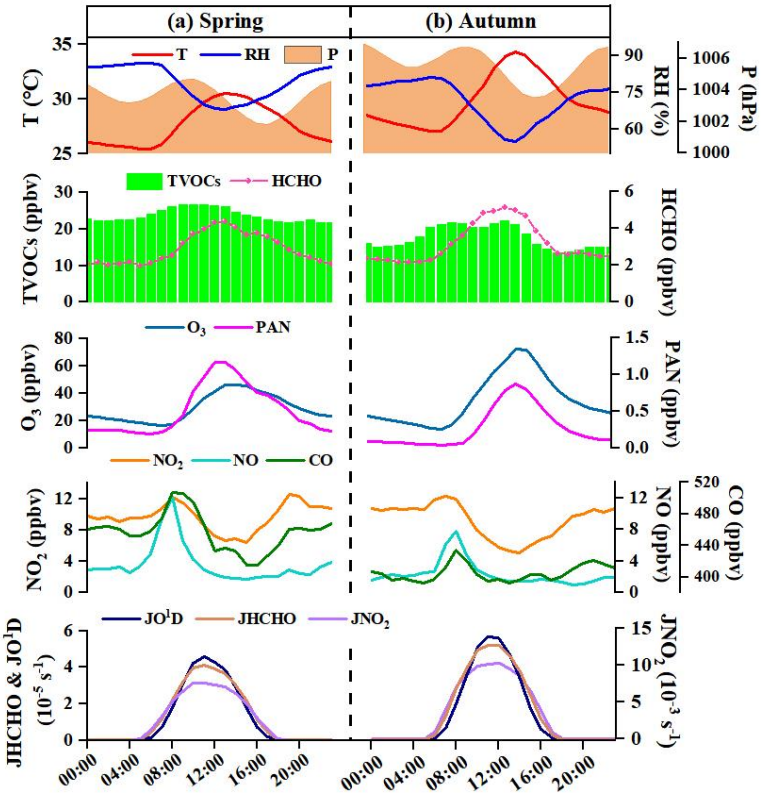

Figure 3. Average diurnal variations of measured HCHO, air pollutants, meteorological parameters, and photolysis rate constants during (a) spring and (b) autumn.

3.2 Source apportionment of HCHO

PMF was used to analyze the primary and secondary sources of HCHO. As shown in Fig. S2, five factors were identified by the PMF model. Factor 1 was characterized by a high load of O_3, which was attributed to intense photochemical processes and secondary formation (Li et al., 2010). Factor 2 has high loadings of 3-methylpentane, iso-pentane, the light hydrocarbons of n/iso-pentane and n/iso-butane, and aromatics. Therefore, factor 2 is defined as the source of vehicle exhaust (Li et al., 2017; Liu et al., 2008). Factor 3 contributed significantly to alkenes and aromatics, such as propene, 1-butene, ethene, and benzene, which were the main VOC species in petrochemical industry (Sinha et al., 2019; Wu et al., 2016; Guven and Olaguer, 2011). This factor was identified as industrial emission. Factor 4 was characterized by a high percentage of isoprene, and was designated as biogenic source (Sindelarova et al., 2022; Na et al., 2004). Factor 5 has high loadings of toluene and 1,2-dichloroethane, which were widely used as industrial solvents and laboratory reagents (Mo et al., 2017). So, factor 5 was identified as solvent usage.

The percentages of different sources to ambient HCHO in spring and autumn was shown in Fig. 4. The

https://doi.org/10.5194/acp-2022-292
Preprint. Discussion started: 17 May 2022

Atmospheric Chemistry and Physics Discussions

contribution of secondary formation (49% in spring and 46% in autumn) to HCHO was the largest, comparable to other urban sites such as Guangzhou (53%) (Ling et al., 2017) and Hong Kong (53%) (Lui et al., 2017). Previous studies have reported that secondary formation was generally the main source of HCHO (34%~70%) (Guven and Olaguer, 2011; Ling et al., 2017; Wang et al., 2017; Zeng et al., 2019). The contribution of HCHO from vehicle exhaust in spring (25%) was higher than that in autumn (20%), partly attributed to the unfavorable diffusion conditions in spring. According to backward trajectories analysis (Fig. S3), air mass (87%) in spring originated from the southwest, which passed through Xiamen downtown areas with large amounts of vehicle exhausts emissions. The variation of biogenic source showed a clear seasonal trend, and contributed 18% in spring and 24% in autumn to the ambient HCHO, which consisted of isoprene levels. The contribution of biogenic source in Xiamen with high vegetation coverage was higher than that in an urban site of Wuhan (9%) (Zeng et al., 2019). The industrial source in autumn was 1.5 times higher than that in spring, which could be attributed to long-range transport from the northeast. Backward trajectories (Fig. S3) in autumn showed 55% air mass transport from the northeast, which brought pollutants from Quanzhou city, an industrial city adjacent to Xiamen. The contributions of solvent usage to HCHO seemed to be minor. The results were similar to those at the urban sites (Zeng et al., 2019). Totally, secondary formation, vehicle exhaust, and biogenic source made significant contributions to HCHO with total contributions of 48%, 23%, and 21%, respectively.

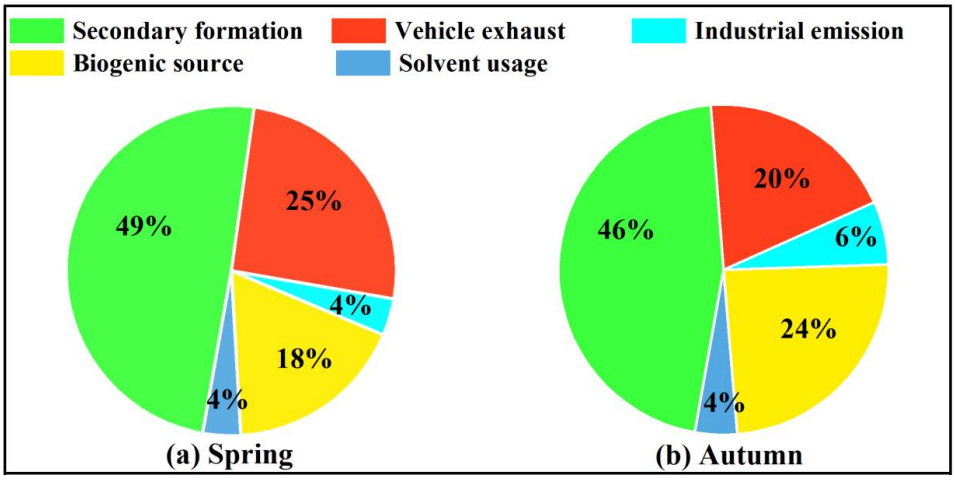

Figure 4. Seasonal variation of various source contributions to HCHO levels in (a) spring and (a) autumn.

https://doi.org/10.5194/acp-2022-292
Preprint. Discussion started: 17 May 2022


Atmospheric Chemistry and Physics Discussions

3.3 HCHO formation mechanisms

3.3.1 HCHO in situ formation pathways

Figure 5 shows the production and loss pathways of HCHO based on OBM-MCM model. HCHO production rates during the daytime (06:00-17:00 LT) in spring and autumn were 1.89±0.99 ppbv h^{-1} and 1.97±1.16 ppbv h^{-1}, while HCHO loss rates were 1.88±1.37 ppbv h^{-1} and 2.47±1.87 ppbv h^{-1}, respectively. The results showed that HCHO loss rates in autumn were higher than that in spring. This could be attributed to the favorable meteorological conditions for photolysis, such as intense solar radiation, high air temperature, and low relative humidity, but relatively low levels of air pollutants in autumn compared to those in spring. The daytime average net production rate of HCHO (NP_{HCHO}) was 0.10±0.37 ppbv h^{-1} in spring, comparable to that in an island of Hong Kong (0.12 ppbv h^{-1}), an urban site (0.18 ppbv h^{-1}) and a roadside site (0.16 ppbv h^{-1}) of Wuhan, but the NP_{HCHO} (–0.40±0.70 ppbv h^{-1}) in autumn was relatively low, due to the increase of HCHO loss rate under the intense solar radiation and relatively low precursor levels to limited HCHO secondary formation (Zhang et al., 2021a; Yang et al., 2020). The NP_{HCHO} reached two peaks at around 07:00 and 16:00 in both seasons (0.47 ppbv h^{-1} in spring and 0.35 ppbv h^{-1} in autumn), and presented the lowest values during 12:00-13:00 LT, when the favorable meteorological conditions made HCHO decomposition more competitive. This result verified that the strong photochemical reaction was conducive to the HCHO production, but also limited the high HCHO value. Previous studies also found that the NP_{HCHO} showed negative values and reached the lowest at noon (Zhang et al., 2021a; Zeng et al., 2019).

The dominant pathway of daytime average HCHO production rate was the RO+O_2 reaction, and the reaction rates were 1.68±0.90 ppbv h^{-1} and 1.71±1.02 ppbv h^{-1}, which accounted for 87% and 85% of all HCHO production pathways in spring and autumn, respectively. After further refinement of the RO+O_2 reactions by classifying different RO first-generation precursors, the CH_3O+O_2 pathway contributed RO+O_2 reaction rates mostly for 65% and 67%, and contributed to total HCHO production rates of 57% and 58% in spring and autumn, respectively. Moreover, RO derived from alkenes and isoprene reacting with O_2 contributed to total HCHO production of 0.41±0.22 ppbv h^{-1} (21%) and 0.11±0.05 ppbv h^{-1} (6%) in spring, and 0.37±0.22 ppbv h^{-1} (18%) and 0.12±0.07 ppbv h^{-1} (6%) in autumn, respectively, and the contributions of RO produced by alkanes and aromatics were less than 2%. The ‘others’ category (detailed reactions showed in Table S7) accounted for 9% and 11% of the total production rate in spring and autumn, respectively. As for the loss pathways of HCHO, the reaction rates of HCHO+OH were 1.01±0.85 ppbv h^{-1} (55%) and 1.47±1.24 ppbv h^{-1} (61%), and the HCHO photolysis was 0.84±0.53 ppbv h^{-1} (45%) and 0.97±0.63 ppbv h^{-1} (39%) in spring and autumn, respectively. It was worth noting that the contributions of HCHO production pathways

https://doi.org/10.5194/acp-2022-292
Preprint. Discussion started: 17 May 2022

Atmospheric Chemistry and Physics Discussions

had minor seasonal variations, while the contributions of HCHO loss pathways in autumn were significantly higher than those in spring. The results implied strong photochemical effects with high yields of ROx radical in autumn (the detailed description of ROx showed in Fig. 9 of Section 3.4.2).

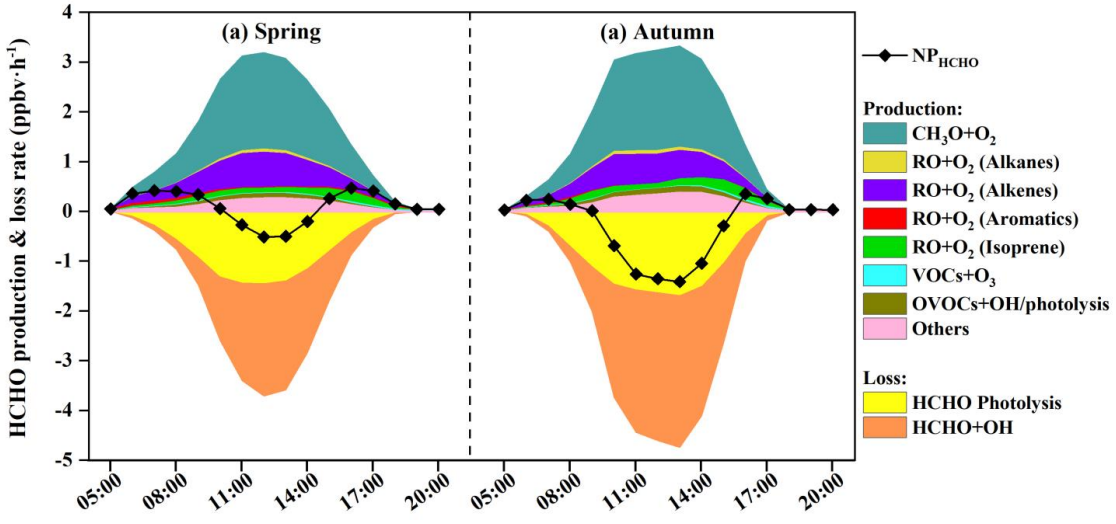

Figure 5. Model-simulated in situ HCHO production rate and loss rate in (a) spring and (b) autumn.

3.3.2 Identification of key precursor species of HCHO

Sensitivity tests based on the OBM-MCM model were furtherly carried out to quantify the potential influence of different precursors on HCHO formation (Liu et al., 2022a; Yang et al., 2020). Figure 6 shows the relative incremental reactivity (RIR) for major groups and specific species of HCHO precursors. HCHO production was highly VOCs-sensitive with positive RIR values, indicating that reducing VOCs emissions might effectively inhibit the HCHO formation in Xiamen. As shown in Fig. 6(a), the formation of HCHO was mainly controlled by alkenes with the largest RIR values in spring (1.19) and autumn (1.05), followed by isoprene (0.58 in spring and 0.78 in autumn), aromatics (0.75 in spring and 0.55 in autumn), and alkanes (0.45 in spring and 0.43 in autumn). The results suggested that both biogenic and anthropogenic emissions influenced the HCHO secondary formation. In addition, the RIR of isoprene in spring was lower than that in autumn, which was attributed to the seasonal characteristics of isoprene concentrations affected by solar radiation and air temperature (Blas et al., 2019).

Based on the explicit mechanism in the OBM-MCM model, HCHO precursors at the species level could be further identified. In this study, the impact of anthropogenic precursors on HCHO was mainly discussed. Alkenes and aromatics made the greatest contributions to HCHO formation among the top 10 VOCs species

https://doi.org/10.5194/acp-2022-292
Preprint. Discussion started: 17 May 2022

Atmospheric Chemistry and Physics Discussions

(Fig. 6(b)). The top 5 species of RIR were propene (0.35 in spring and 0.31 in autumn), ethene (0.35 and 0.18), toluene (0.27 and 0.17), m/p-xylene (0.21 and 0.10), and trans-2-butene (0.15 and 0.15), related to their concentrations in different seasons (Table S5). In addition, for the contributions of anthropogenic emissions to HCHO formation, vehicle exhaust and biomass burning were the dominant contributors, followed by solvent usage (Ling et al., 2017; Sinha et al., 2019). These results were consistent with HCHO source apportionment of PMF in Section 3.2, and also with previous studies in Wuhan and Hong Kong (Zeng et al., 2019; Yang et al., 2020).

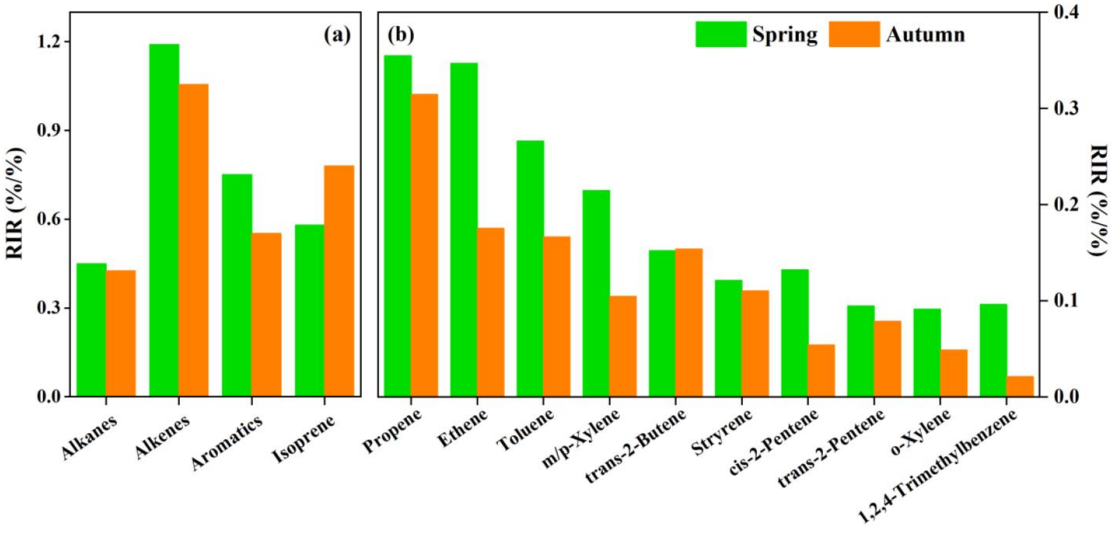

Figure 6. The OBM-MCM calculated relative incremental reactivity (RIR) for (a) major HCHO precursor groups and (b) top 10 specific species in spring and autumn during the daytime (06:00-17:00 LT).

3.4. Contribution of HCHO to atmospheric photochemistry

3.4.1 Impacts on atmospheric oxidation

The atmospheric oxidation capacity (AOC) is a crucial aspect of exploring the complex atmospheric photochemistry processes, reflecting the essential driving force in the loss of primary components and the production of secondary pollutants in tropospheric chemistry (Chen et al., 2020). AOC was defined as the sum of oxidation rates in converting primary pollutants (CO, VOCs, etc.) into secondary pollutants by the major oxidants (i.e., OH, NO_3, O_3) (Xue et al., 2016). Figure 7 shows the diurnal patterns of the model-calculated AOC during the observation period. The daily maximum AOC was shown at around 12:00 LT with levels of 1.24×10^8 molecules cm^{-3} s^{-1} in spring and 1.48×10^8 molecules cm^{-3} s^{-1}in autumn, which was comparable to that in the suburban site of the YRD region (1.24×10^8 molecules cm^{-3} s^{-1}), higher than that in a regional

https://doi.org/10.5194/acp-2022-292
Preprint. Discussion started: 17 May 2022

Atmospheric Chemistry and Physics Discussions

background in Hong Kong (6.2 × 10^7 molecules cm^{-3} s^{-1}) and a rural site with much low pollution sources in Berlin (1.4× 10^7 molecules cm^{-3} s^{-1}), but lower than that in some cities, such as Santiago (3.2×10^8 molecules cm^{-3} s^{-1}) (Zhang et al., 2021a; Xue et al., 2016; Geyer et al., 2001; Zhu et al., 2020). The AOC levels in different regions were mainly controlled by the precursors and photochemical conditions, such as solar radiation and air temperature. As Fig. 7 shows, the OH played a dominant role in contribution to AOC during the daytime, accounting for around 97% of total AOC, then O_3 and NO_3 contributed 2% and 3% in both seasons. During the nighttime, NO_3 (71% in spring and 66% in autumn) contributed the most, followed by OH (15% and 21%) and O_3 (14% and 13%). In particular, the AOC by NO_3 contributed to the maximum at around 19:00 LT of 84% in spring and 71% in autumn, when relatively high concentrations of O_3 and NO_2 with weak solar radiation accelerated the formation and accumulation of NO_3 (Fig. 3) (Rollins et al., 2012; Chen et al., 2020). The AOC levels in autumn were 1.20~1.43 times higher than that in spring, due to the favorable photochemical conditions. And, the main contribution of AOC was OH radicals, which greatly caused the production of secondary pollutants.

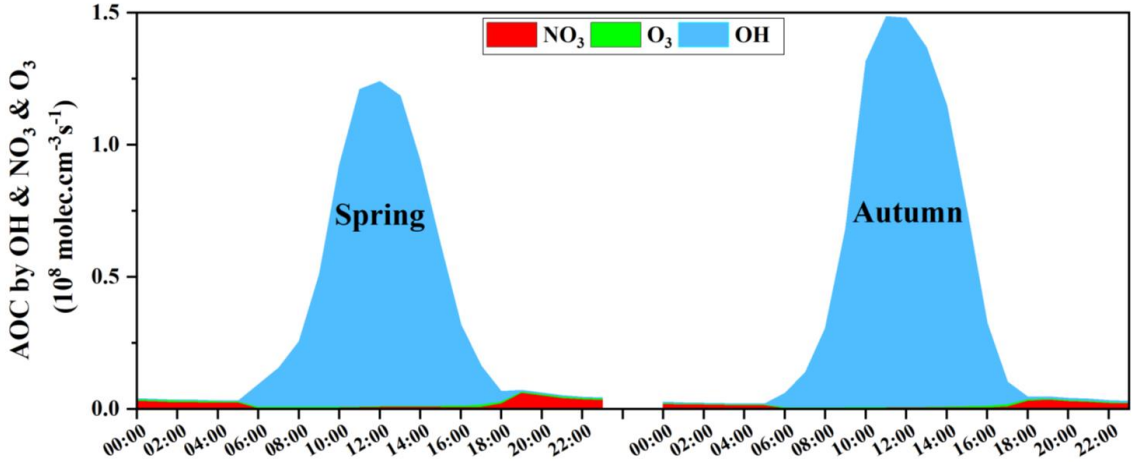

Figure 7. The model-calculated atmospheric oxidation capacity (AOC) in spring and autumn.

OH reactivity was used to compare the importance of different reactants to the OH loss, and the model-calculated OH reactivity in spring and autumn were shown in Fig. 8. The daytime average OH reactivities were 12.82±2.73 s^{-1} in spring and 10.00±2.30 s^{-1} in autumn, which were much lower than those in polluted urban regions, but higher than that in remote or background sites (Lou et al., 2010; Kovacs et al., 2003; Ren et al., 2005; Zhu et al., 2020). Here, the OH reactivity includes the OH oxidation of both measured species (such as NOx, CO, C_2-C_{10} hydrocarbons, and measured carbonyls) and modeled compounds (mainly including

https://doi.org/10.5194/acp-2022-292
Preprint. Discussion started: 17 May 2022

Atmospheric Chemistry and Physics Discussions

379 unmeasured higher OVOCs), and the OH reactivity from the measured compounds accounted for the majority
380 of the total OH reactivity, thus the OH reactivity from the modeled results might be subject to some uncertainty
381 due to the lack of direct observations. Compared to measured OH reactivity in other regions of China, the
382 daily median OH reactivity was 20±11 s^{-1} at an urban site in Beijing and 31±20 s^{-1} at a suburban site in Heshan
383 of Guangdong Province (Yang et al., 2016, 2017). At a rural site in Wangdu, measured OH reactivity values
384 ranged between 10 and 20 s^{-1}, and the median value during the daytime was 12.4 s^{-1} (Fuchs et al., 2017). The
385 simulated OH reactivities in our study were within the measured range of other sites in China. Oxygenated
386 volatile organic compounds (OVOCs, 30% in spring and 31% in autumn), NO_2 (27% and 31%), and CO (28%
387 and 28%) showed large fractions of OH reactivity, followed by NO (6% and 5%), alkenes with relatively high
388 reactivity compared with hydrocarbons (6% and 4%), alkanes (3% and 3%), and aromatics (3% and 2%). It
389 should be noted that HCHO accounted for 28% in spring and 34% in autumn of the OH reactivity by OVOCs,
390 and contributed 8% in spring and 10% in autumn to the total OH reactivity, elucidating the significance of
391 HCHO in photochemistry. A previous study also showed the importance of HCHO in atmospheric radicals of
392 HO_2 and O_3 formation (Zeng et al., 2019).
393

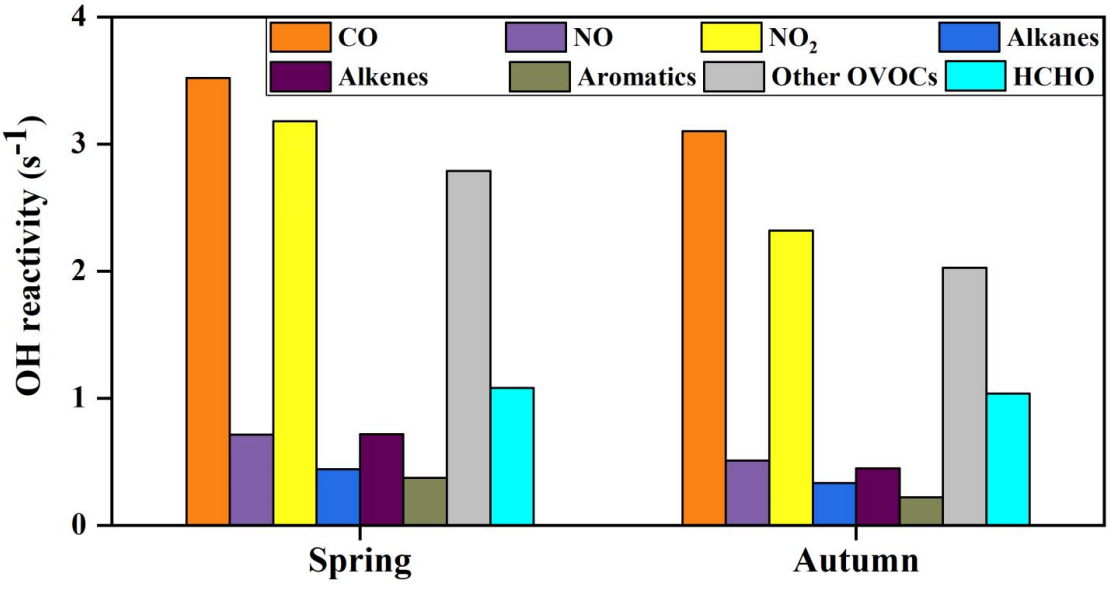

394
395 **Figure 8. The model-calculated OH reactivity in spring and autumn during the daytime (06:00-17:00**
396 **LT).**
397
398
399
400

https://doi.org/10.5194/acp-2022-292
Preprint. Discussion started: 17 May 2022


Atmospheric Chemistry and Physics Discussions

3.4.2 Impacts on the diurnal patterns of radicals

HCHO modulates O_3 formation mainly by controlling the radical recycling in the troposphere (Zeng et al., 2019). To furtherly quantify the changes in ROx chemistry and O_3 formation in response to HCHO chemistry, two parallel scenarios were conducted through OBM-MCM model. One scenario was run with all MCM mechanism defined as AS, and the other was run with the HCHO mechanism disabled in MCM mechanism defined as DS. The loss pathways of HCHO (mainly including its photolysis and oxidation with OH radical producing HO_2 radical, detailed information in Section 3.3.1) played the key role in the most significant impacts of HCHO on atmospheric photochemistry, thus the HCHO loss pathways were disabled in DS scenario.

Figure 9 shows the diurnal trends of OH, HO_2, and RO_2 radicals in model scenarios of AS and DS. The ROx showed a significant decline in DS compared to AS. Both the levels and the differences in ROx between AS and DS were higher in autumn than those in spring, which was caused by the intensity of solar radiation (according to the photolysis frequencies in Fig. 9). Anymore, Figure S4 showed the key simulated production and loss rates of ROx, and we found only the ROx loss rate of $OH+NO_2 \rightarrow RO_2$ in spring (2.06 ppbv h^{-1}) was significantly higher than that in autumn (1.79 ppbv h^{-1}), while the other production and loss rates in spring were lower or comparable than those in autumn. This result could be explained as that high NO_2 in spring consumed OH much resulting in low OH level, then low OH concentration suppressed the RO_2 production through OH+VOCs reactions leading to less RO production via RO_2+NO pathways in spring. These discussions also furtherly testified to the seasonal differences in HCHO+OH reaction rate in Section 3.3.1. For AS, the maximum daily values of OH, HO_2, and RO_2 concentrations in spring were 1.52×10^7, 6.17×10^8, and 3.08×10^8 molecule·cm^{-3}, and those in autumn were 2.35×10^7, 1.12×10^9, and 5.09×10^8 molecule·cm^{-3}, respectively. The measured values of ROx in Xiamen were lacking, and we compared the measured values in other regions of China. The maximum daily values of OH and HO_2 were in the range of $(4–17)\times10^6$ molecule cm^{-3} and $(2–24)\times10^8$ molecule cm^{-3} at both the suburban site and rural site during summer in the North China Plain, respectively (Lu et al., 2012; Tan et al., 2017). The air temperature of Xiamen in autumn was very high and close to that of summer, thus the simulated OH and HO_2 concentrations in our study were comparable with the measured results of other places in China. Anymore, previous studies verified that modeled and measured OH agree well when NO mixing ratios were above 1 ppbv, and a continuously increasing underprediction of the observed OH was found towards lower NO concentrations (Lu et al., 2012). The daytime average difference values of OH, HO_2, and RO_2 between AS and DS in spring were 1.81×10^6, 1.10×10^8, and 0.32×10^8 molecule·cm^{-3}, while those in autumn were 1.82×10^6, 1.89×10^8, and 0.40×10^8

https://doi.org/10.5194/acp-2022-292
Preprint. Discussion started: 17 May 2022

Atmospheric Chemistry and Physics Discussions

molecule·cm^{-3}, respectively (Fig. 9). The importance of HCHO in ROx chemistry indicated the necessity to study the inherent ROx recycling mechanisms.

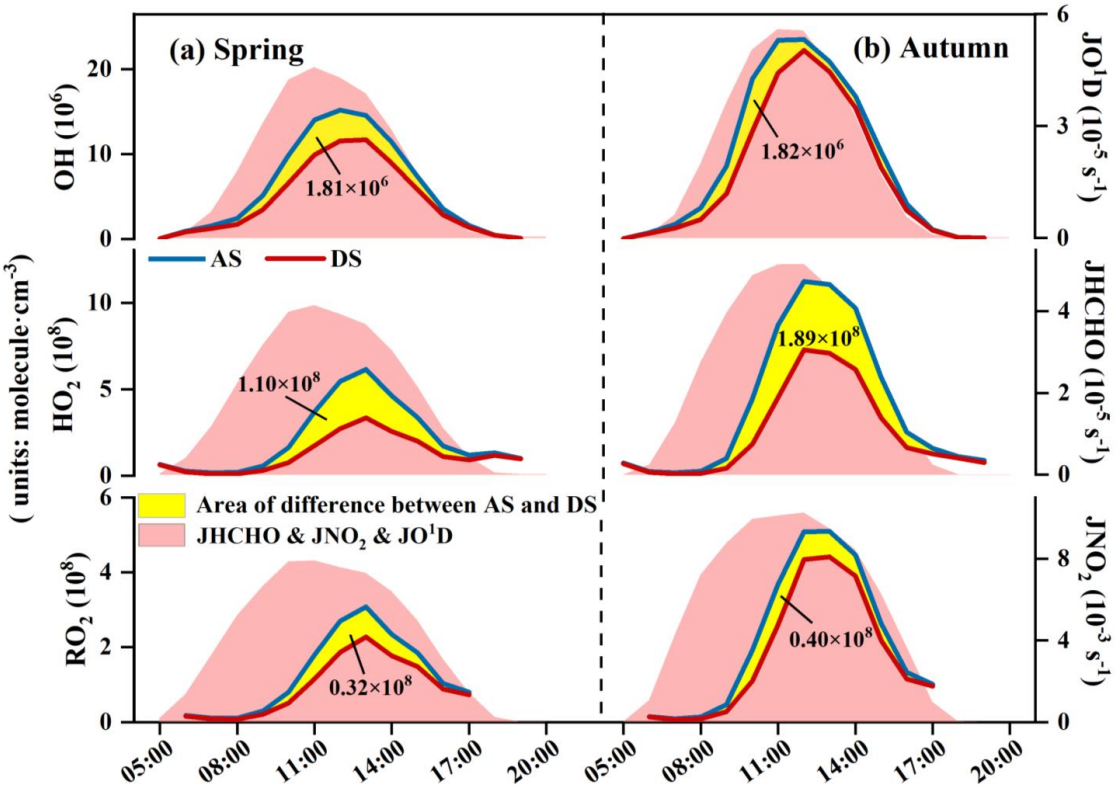

Figure 9. The diurnal patterns and differences of OH, HO_2, and RO_2 radicals in model scenarios of AS and DS in (a) spring and (b) autumn. AS scenario was run with all MCM mechanism, and DS scenario was run with the HCHO mechanism disabled in MCM mechanism.

3.4.3 Impacts on the formation pathways of radicals

To investigate the chain effect of HCHO on ROx cycling, the formation pathways of radicals were also analyzed by the OBM model in DS and AS scenarios. Fig. 10 shows the differences in ROx production pathways in model scenarios of AS and DS. The daytime average OH decreased by 25 % in spring and 16 % in autumn when HCHO mechanism were disabled. HO_2+NO, O_3 photolysis, and HONO photolysis were critical pathways for OH production, which were 7.78, 0.71, 0.53 ppbv h^{-1} in spring and 8.57, 1.06, 0.45 ppbv h^{-1} in autumn, respectively. The reaction rates of O_3+VOCs, HNO_3 photolysis, H_2O_2 photolysis, and OVOCs photolysis were all below 0.02 ppbv h^{-1}, and their changes between AS and DS could be ignored. In Table S8, disabling HCHO mechanism in DS mainly slowed down the OH production pathway of HO_2+NO, which decreased by 2.75 ppbv h^{-1} (35 %) in spring and 2.61 ppbv h^{-1} (30%). The decrease of O_3 photolysis from AS

https://doi.org/10.5194/acp-2022-292
Preprint. Discussion started: 17 May 2022


Atmospheric Chemistry and Physics Discussions

to DS was 0.06 ppbv h^{-1} (9% in spring) and 0.08 ppbv h^{-1} (8%) in autumn, and the decrease of HONO photolysis from AS to DS was 0.06 ppbv h^{-1} (12%) in spring and 0.04 ppbv h^{-1} (9%) in autumn. The daytime average HO_2 decreased by 45% in spring and 40% in autumn between AS and DS. Except for the O_3+VOCs, the other HO_2 production pathways of OH+CO, RO_2+NO, OH+VOCs, HCHO photolysis, and OVOCs photolysis showed relatively high contributions with production rates of 2.91, 1.77, 1.30, 0.79, 0.38 ppbv h^{-1} in spring and 3.93, 1.82, 1.83, 0.92, 0.36 ppbv h^{-1} in autumn, respectively. Among them, the difference in the HCHO photolysis between AS and DS was most with 100% reduction of HO_2 production, followed by OH+VOCs (84% in both seasons), OH+CO (26% in spring and 17% in autumn), RO_2+NO (11% and 6%), and OVOCs photolysis (2% and 1%). The daytime average RO_2 decreased by 26 % in spring and 19 % in autumn from AS to DS. Similar to the analysis above, OH+VOCs (2.75 ppbv h^{-1} in spring and 2.74 ppbv h^{-1} in autumn) and OVOCs photolysis (0.33 ppbv h^{-1} and 0.34 ppbv h^{-1}) represented the remarkable importance on RO_2 production. The deletion of the HCHO loss reactions also led to a decrease in the daytime reaction rate of OH+VOCs by 0.53 ppbv h^{-1} (19%) in spring and 0.29 ppbv h^{-1} (10%) in autumn. The decreasing percentages of OVOCs photolysis were 5% in both seasons, and the changes of NO_3+VOCs and O_3+VOCs were slight. The differences in ROx concentration between AS and DS in autumn were higher than that in spring, but the decrease percentage in autumn was lower than that in spring due to the ROx levels. Meanwhile, the ROx production rates in autumn were lower than those in spring due to the limited VOCs levels.

HCHO photolysis was the major pathway for HO_2 production, thus the differences in HO_2 between AS and DS were the highest, followed by RO_2 and OH. Deleting the reactions of HCHO on HO_2 production pathway would decrease the OH production due to the key reaction of HO_2+NO→OH, as a result, the RO_2 production would be weakened due to the critical production pathway of OH+VOCs→HO_2. In general, the decreases in OH and RO_2 concentrations caused by HCHO were mainly dominated by the reduction of radical propagation efficiencies. Meanwhile, in addition to the HCHO photolysis, radical propagation also played a very important role in HO_2 production. In Zeng et al. (2019) study, HCHO had a non-negligible contribution to HO_2 production, and the HO_2 production rates from HCHO photochemical reactions accounted for 15% of total HO_2 production rates.

https://doi.org/10.5194/acp-2022-292
Preprint. Discussion started: 17 May 2022

Atmospheric Chemistry and Physics Discussions

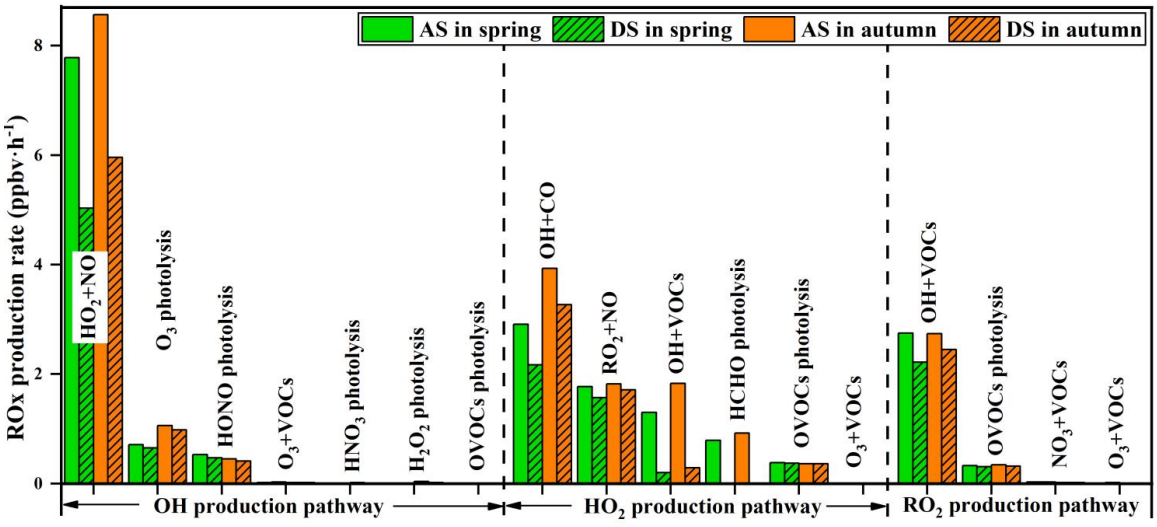

Figure 10. The average daytime (06:00-17:00) production rates of OH, HO_2, and RO_2 in model scenarios of AS and DS. AS scenario was run with all MCM mechanism, and DS scenario was run with the HCHO mechanism disabled in MCM mechanism.

3.4.4 Impacts on the formation of O_3

To investigate the impacts of HCHO on O_3 formation during the observation period, the detailed O_3 production and loss pathways in both AS and DS were quantified (Fig. 11 and Table 1). The daytime production rates of HO_2+NO and RO_2+NO in AS were 7.78 and 2.96 ppbv h^{-1} in spring and 8.57 and 2.87 ppbv h^{-1} in autumn, accounting for 72% and 28% in spring and 75% and 25% in autumn of the total O_3 production, respectively. Meanwhile, OH+NO_2 was the predominant O_3 loss reaction with 1.93 ppbv h^{-1} (60%) in spring and 1.79 ppbv h^{-1} (60%) in autumn, followed by O_3 photolysis (22% in spring and 29% in autumn), RO_2+NO_2 (8% and 7%), O_3+HO_2 (3% and 8%), and O_3+OH (3% and 6%), while the contributions of O_3+VOCs and NO_3+VOCs pathways were very limited.

https://doi.org/10.5194/acp-2022-292
Preprint. Discussion started: 17 May 2022

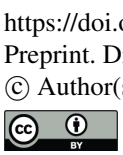

Atmospheric Chemistry and Physics Discussions

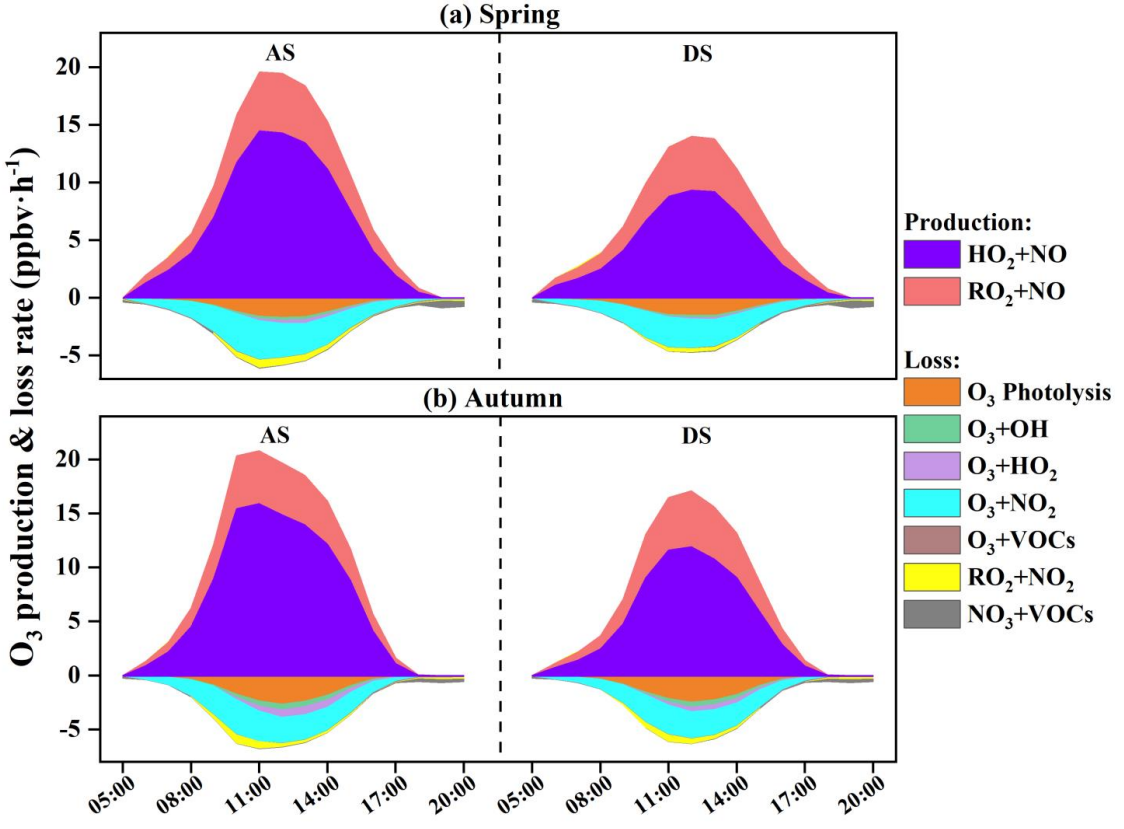

Figure 11. Simulated profiles of O_3 mechanism in AS and DS in (a) spring and (b) autumn. AS scenario was run with all MCM mechanism, and DS scenario was run with the HCHO mechanism disabled in MCM mechanism.

According to the differences between AS and DS, disabling HCHO mechanism could reduce the production rates of HO_2+NO by 2.75 ppbv h^{-1} (35%) in spring and 2.61 ppbv h^{-1} (30%) in autumn, and decrease RO_2+NO by 0.39 ppbv h^{-1} (13%) in spring and 0.18 ppbv h^{-1} (6%) in autumn (Table 1). About the O_3 loss pathways, the differences mainly reduced the rates of OH+NO_2 by 0.40 ppbv h^{-1} (21%) in spring and 0.24 ppbv h^{-1} (13%) in autumn, decreased O_3 photolysis by 0.06 (9%) in spring and 0.08 ppbv h^{-1} (8%) in autumn, weakened RO_2+NO_2 by 0.16 ppbv h^{-1} (62%) in spring and 0.05 ppbv h^{-1} (19%) in autumn, lessened O_3+HO_2 by 0.06 ppbv h^{-1} (50%) in spring and 0.12 ppbv h^{-1} (43%) in autumn, and dropped O_3+OH by 0.03 ppbv h^{-1} (31%) in spring and 0.04 ppbv h^{-1} (19%) in autumn. The daytime average values of net O_3 production rates decreased by 32% in spring and 29% in autumn, and the peak net O_3 rate decreased by 32% in spring and 23% in autumn. Other studies indicated that the peak net O_3 rates in summer were reduced by 31% in a roadside site, 17% in a typical urban site, and 13% in a suburban site through diminishing HCHO (Zeng et al., 2019). When the HCHO mechanism was disabled, HO_2+NO, RO_2+NO_2, O_3+HO_2, O_3+OH, and OH+NO_2

https://doi.org/10.5194/acp-2022-292
Preprint. Discussion started: 17 May 2022

Atmospheric Chemistry and Physics Discussions

showed significant changes. These reactions were all radical propagation pathways, which were consistent with the results in Section 3.4.2. Therefore, the results highlighted and quantified the important impacts of HCHO on O_3 formation in the southeast coastal area.

Table 1. The average daytime (06:00-17:00) production rates, loss rates, and differences of O_3 in model scenarios of AS and DS. AS scenario was run with all MCM mechanism, and DS scenario was run with the HCHO mechanism disabled in MCM mechanism.

Reactions	Spring			Autumn		
	AS	DS	Difference	AS	DS	Difference
O_3 production rate (ppbv h^{-1})						
HO_2+NO	7.78	5.03	35%	8.57	5.96	30%
RO_2+NO	2.96	2.57	13%	2.87	2.69	6%
O_3 loss rate (ppbv h^{-1})						
OH+NO_2	1.93	1.53	21%	1.79	1.55	13%
O_3 photolysis	0.71	0.65	9%	1.06	0.98	8%
RO_2+NO_2	0.26	0.10	62%	0.25	0.20	19%
O_3+HO_2	0.11	0.05	50%	0.28	0.16	43%
O_3+OH	0.11	0.08	31%	0.22	0.18	19%
Net O_3 production rate	7.53	5.09	32%	7.75	5.49	29%

4 Conclusions

Combined field observations with model analyses were carried out in spring and autumn, when photochemical pollution events frequently appeared in a coastal city of southeast China. We found that the average levels of secondary products in autumn, such as O_3 and HCHO, were higher than those in spring, relating to the intense photochemical reaction and meteorological conditions, although the concentrations of NOx and VOCs in autumn were lower than those in spring. HCHO from secondary formation made the largest contributions to ambient HCHO, followed by the primary sources of vehicle exhaust and biogenic emission. The sensitivity analysis found that alkenes and aromatics were the most important precursors to HCHO from secondary formation. Meanwhile, the top 5 precursors at the species level contributing to HCHO were propene, ethene, toluene, m/p-xylene, and trans-2-butene, which were mainly emitted from combustion sources and solvents use. The results indicated that the reduction of the two sources could effectively decrease both primary and secondary sources of HCHO. Based on the analysis of disabling HCHO mechanism, we verified that HCHO contributed to the AOC of 8% in spring and 10% in autumn, and decreased the concentrations of ROx, reflecting the significance of HCHO in photochemistry. The daytime average values of net O_3 production rates decreased by 32% in spring and 29% in autumn by disabling the HCHO mechanism. For the O_3 formation mechanism, disabling HCHO mechanism reduced the production rates of HO_2+NO and RO_2+NO, and lessened the O_3 loss pathways of OH+NO_2, RO_2+NO_2, O_3+HO_2, and O_3+OH, indicating that the HCHO affected O_3 formation mechanism mainly by controlling the efficiencies of radical propagation. This study

https://doi.org/10.5194/acp-2022-292
Preprint. Discussion started: 17 May 2022


Atmospheric Chemistry and Physics Discussions

536 gives a scientific reference for HCHO source, formation pathway, and its contribution to the photochemistry
537 and further understanding of ozone pollution prevention in the coastal region.
538
539 **Code and Data availability**
540 The observation data at this site are available from the authors upon request.
541
542 **Authorship Contribution Statement**
543 Taotao Liu collected the data, contributed to the data analysis and performed chemical modeling analyses
544 of OBM-MCM, and wrote the paper. Jinsheng Chen designed the manuscript and supported funding of
545 observation and research. Yiling Lin collected the data and contributed to the PMF analysis. Youwei Hong
546 revised the manuscript. Gaojie Chen, Chen Yang, Lingling Xu, Mengren Li, Xiaolong Fan, Yanting Chen,
547 Liqian Yin, Yuping Chen, Xiaoting Ji, Ziyi Lin contributed to discussions of results. Fuwang Zhang and Hong
548 Wang provided part of the data in Xiamen.
549
550 **Competing interests**
551 The contact author has declared that neither they nor their co-authors have any competing interests.
552
553 **Acknowledgment**
554 This study was funded by the Cultivating Project of Strategic Priority Research Program of Chinese
555 Academy of Sciences (XDPB1903), the National Key Research and Development Program (2016YFC02005),
556 the National Natural Science Foundation of China (U1405235), the foreign cooperation project of Fujian
557 Province (2020I0038), the Xiamen Youth Innovation Fund Project (3502Z20206094), the FJIRSM&IUE Joint
558 Research Fund (RHZX-2019-006), center for Excellence in Regional Atmospheric Environment project
559 (E0L1B20201), Xiamen Atmospheric Environment Observation and Research Station of Fujian Province, and
560 Fujian Key Laboratory of Atmospheric Ozone Pollution Prevention (Institute of Urban Environment, Chinese
561 Academy of Sciences).

https://doi.org/10.5194/acp-2022-292
Preprint. Discussion started: 17 May 2022

Atmospheric Chemistry and Physics Discussions

562 **References:**

563 Anderson, D., Nicely, J., Wolfe, G., Hanisco, T., Salawitch, R., Canty, T., Dickerson, R., Apel, E., Baidar, S.,
564 Bannan, T., Blake, N. J., Chen, D., Dix, B., Fernandez, R. P., Hall, S. R., Hornbrook, R. S., Huey, L. G., Josse,
565 B., Jöckel, P., Kinnison, D. E., Koenig, T. K., Breton, M. L., Marécal, V., Morgenstern, O., Oman, L. D., Pan,
566 L. L., Percival, C., Plummer, D., Revell, L. E., Rozanov, E., Saiz-Lopez, A., Stenke, A., Sudo, K., Tilmes, S.,
567 Ullmann, K., Volkamer, R., Weinheimer, A. J., and Zeng, G.: Formaldehyde in the tropical western Pacific:
568 Chemical sources and sinks, convective transport, and representation in CAM-Chem and the CCMI models,
569 J. Geophys. Res.-Atmos., 122, 11201–11226, https://doi.org/10.1002/2016JD026121, 2017.

570 Bao, J., Li, H., Wu, Z., Zhang, X., Zhang, H., Li, Y., Qian, J., Chen, J., and Deng, L.: Atmospheric carbonyls
571 in a heavy ozone pollution episode at a metropolis in Southwest China: Characteristics, health risk assessment,
572 sources analysis, J Environ Sci (China), 113, 40-54, 10.1016/j.jes.2021.05.029, 2022.

573 Blas, M., Ibanez, P., Garcia, J. A., Gomez, M. C., Navazo, M., Alonso, L., Durana, N., Iza, J., Gangoiti, G.,
574 and de Camara, E. S.: Summertime high resolution variability of atmospheric formaldehyde and non-methane
575 volatile organic compounds in a rural background area, Sci Total Environ, 647, 862-877,
576 10.1016/j.scitotenv.2018.07.411, 2019.

577 Brown, S.G., Eberly, S., Paatero, P., Norris, G.A.: Methods for estimating uncertainty in PMF solutions:
578 examples with ambient air and water quality data and guidance on reporting PMF results. Sci. Total Environ.
579 518–519, 626–635, 2015.

580 Chen, T., Xue, L., Zheng, P., Zhang, Y., Liu, Y., Sun, J., Han, G., Li, H., Zhang, X., Li, Y., Li, H., Dong, C.,
581 Xu, F., Zhang, Q., and Wang, W.: Volatile organic compounds and ozone air pollution in an oil production
582 region in northern China, Atmos. Chem. Phys. 20, 7069-7086, 10.5194/acp-20-7069-2020, 2020.

583 Chen, W. T., Shao, M., Lu, S. H., Wang, M., Zeng, L. M., Yuan, B., and Liu, Y.: Understanding primary and
584 secondary sources of ambient carbonyl compounds in Beijing using the PMF model, Atmos. Chem. Phys., 14,
585 3047-3062, 10.5194/acp-14-3047-2014, 2014.

586 Edwards, P.M., Brown, S.S., Roberts, J.M., Ahmadov, R., Banta, R.M., deGouw, J.A., Dube, W.P., Field, R.A.,
587 Flynn, J.H., Gilman, J.B., Graus, M., Helmig, D., Koss, A., Langford, A.O., Lefer, B.L., Lerner, B.M., Li, R.,
588 Li, S.M., McKeen, S.A., Murphy, S.M., Parrish, D.D., Senff, C.J., Soltis, J., Stutz, J., Sweeney, C., Thompson,
589 C.R., Trainer, M.K., Tsai, C., Veres, P.R., Washenfelder, R.A., Warneke, C., Wild, R.J., Young, C.J., Yuan, B.,
590 Zamora, R.: High winter ozone pollution from carbonyl photolysis in an oil and gas basin. Nature, 514, 351–
591 354, 2014.

592 Fuchs, H., Tan, Z., Lu, K., Bohn, B., Broch, S., Brown, S. S., Dong, H., Gomm, S., Häseler, R., He, L.,
593 Hofzumahaus, A., Holland, F., Li, X., Liu, Y., Lu, S., Min, K.-E., Rohrer, F., Shao, M., Wang, B., Wang, M.,
594 Wu, Y., Zeng, L., Zhang, Y., Wahner, A., and Zhang, Y.: OH reactivity at a rural site (Wangdu) in the North
595 China Plain: contributions from OH reactants and experimental OH budget, Atmos. Chem. Phys., 17, 645-
596 661, 10.5194/acp-17-645-2017, 2017.

597 Geyer, A., Alicke, B., Konrad, S., Schmitz, T., Stutz, J., and Platt, U.: Chemistry and oxidation capacity of the
598 nitrate radical in the continental boundary layer near Berlin, J. Geophys. Res., 106, 8013-8025,
599 10.1029/2000jd900681, 2001.

600 Guven, B. and Olaguer, E. P.: Ambient formaldehyde source attribution in Houston during TexAQS II and
601 TRAMP, Atmos. Environ., 45, 4272-4280, 10.1016/j.atmosenv.2011.04.079, 2011.

https://doi.org/10.5194/acp-2022-292
Preprint. Discussion started: 17 May 2022


Atmospheric Chemistry and Physics Discussions

He, Z., Zhang, X., Li, Y., Zhong, X., Li, H., Gao, R., and Li, J.: Characterizing carbonyl compounds and their sources in Fuzhou ambient air, southeast of China, PeerJ, 8, e10227, 10.7717/peerj.10227, 2020.

Hu, B., Duan, J., Hong, Y., Xu, L., Li, M., Bian, Y., Qin, M., Fang, W., Xie, P., and Chen, J.: Exploration of the atmospheric chemistry of nitrous acid in a coastal city of southeastern China: results from measurements across four seasons, Atmos Chem and Phys, 22, 371-393, 10.5194/acp-22-371-2022, 2022.

Jenkin, M. E., Saunders, S. M., Wagner, V., and Pilling, M. J.: Protocol for the development of the Master Chemical Mechanism, MCM v3 (Part B): tropospheric degradation of aromatic volatile organic compounds, Atmos. Chem. Phys., 3, 181–193, https://doi.org/10.5194/acp-3-181-2003, 2003.

Kovacs, T. A., Brune, W. H., Harder, H., Martinez, M., Simpas, J. B., Frost, G. J., Williams, E., Jobson, T., Stroud, C., Young, V., Fried, A., and Wert, B.: Direct measurements of urban OH reactivity during Nashville SOS in summer 1999, J. of Environ. Monitor., 5, 68-74, 10.1039/b204339d, 2003.

Li, B., Ho, S. S. H., Xue, Y., Huang, Y., Wang, L., Cheng, Y., Dai, W., Zhong, H., Cao, J., and Lee, S.: Characterizations of volatile organic compounds (VOCs) from vehicular emissions at roadside environment: The first comprehensive study in Northwestern China, Atmos. Environ., 161, 1-12, 10.1016/j.atmosenv.2017.04.029, 2017.

Li, X., Rohrer, F., Brauers, T., Hofzumahaus, A., Lu, K., Shao, M., Zhang, Y. H., and Wahner, A.: Modeling of HCHO and CHOCHO at a semi-rural site in southern China during the PRIDE-PRD2006 campaign, Atmos. Chem. Phys. 14, 12291-12305, 10.5194/acp-14-12291-2014, 2014.

Li, Y., Shao, M., Lu, S., Chang, C.-C., and Dasgupta, P. K.: Variations and sources of ambient formaldehyde for the 2008 Beijing Olympic games, Atmos. Environ., 44, 2632-2639, 10.1016/j.atmosenv.2010.03.045, 2010.

Li, Z., Xue, L., Yang, X., Zha, Q., Tham, Y. J., Yan, C., Louie, P. K. K., Luk, C. W. Y., Wang, T., and Wang, W.: Oxidizing capacity of the rural atmosphere in Hong Kong, Southern China, Sci Total Environ, 612, 1114-1122, 10.1016/j.scitotenv.2017.08.310, 2018.

Ling, Z. H., Zhao, J., Fan, S. J., and Wang, X. M.: Sources of formaldehyde and their contributions to photochemical O_3 formation at an urban site in the Pearl River Delta, southern China, Chemosphere, 168, 1293-1301, 10.1016/j.chemosphere.2016.11.140, 2017.

Liu, T., Chen, G., Chen, J., Xu, L., Li, M., Hong, Y., Chen, Y., Ji, X., Yang, C., Chen, Y., Huang, W., Huang, Q., and Wang, H.: Seasonal characteristics of atmospheric peroxyacetyl nitrate (PAN) in a coastal city of Southeast China: Explanatory factors and photochemical effects, Atmos. Chem. Phys., 22, 4339-4353, 10.5194/acp-22-4339-2022, 2022a.

Liu, T., Hong, Y., Li, M., Xu, L., Chen, J., Bian, Y., Yang, C., Dan, Y., Zhang, Y., Xue, L., Zhao, M., Huang, Z., and Wang, H.: Atmospheric oxidation capacity and ozone pollution mechanism in a coastal city of southeastern China: analysis of a typical photochemical episode by an observation-based model, Atmos. Chem. Phys., 22, 2173-2190, 10.5194/acp-22-2173-2022, 2022b.

Liu, Y., Shao, M., Fu, L., Lu, S., Zeng, L., and Tang, D.: Source profiles of volatile organic compounds (VOCs) measured in China: Part I, Atmos. Environ., 42, 6247-6260, 10.1016/j.atmosenv.2008.01.070, 2008.

Liu, Y., Yuan, B., Li, X., Shao, M., Lu, S., Li, Y., Chang, C. C., Wang, Z., Hu, W., Huang, X., He, L., Zeng, L., Hu, M., and Zhu, T.: Impact of pollution controls in Beijing on atmospheric oxygenated volatile organic compounds (OVOCs) during the 2008 Olympic Games: observation and modeling implications, Atmos. Chem. Phys. 15, 3045-3062, 10.5194/acp-15-3045-2015, 2015.

https://doi.org/10.5194/acp-2022-292
Preprint. Discussion started: 17 May 2022

642 Lou, S., Holland, F., Rohrer, F., Lu, K., Bohn, B., Brauers, T., Chang, C. C., Fuchs, H., Haeseler, R., Kita, K.,
643 Kondo, Y., Li, X., Shao, M., Zeng, L., Wahner, A., Zhang, Y., Wang, W., and Hofzumahaus, A.: Atmospheric
644 OH reactivities in the Pearl River Delta - China in summer 2006: measurement and model results, Atmos.
645 Chem. Phys., 10, 11243-11260, 10.5194/acp-10-11243-2010, 2010.

646 Lowe, D. C. and Schmidt, U.: Formaldehyde (HCHO) measurements in the nonurban atmosphere, J. Geophys.
647 Res.-Oceans, 88, 10844–10858, https://doi.org/10.1029/JC088iC15p10844, 1983.

648 Lu, K. D, Rohrer F., Holland F., Fuchs H., Bohn B., Brauers T., Chang C. C., Häseler R., Hu M., Kita K.,
649 Kondo, Y., Li, X., Lou, S. R., Nehr, S., Shao, M., Zeng, L. M., Wahner, A., Zhang, Y. H., Hofzumahaus, A.:
650 Observation and modelling of OH and HO_2 concentrations in the Pearl River Delta 2006: a missing OH source
651 in a VOC rich atmosphere. Atmos. Chem. Phys., 12(3), 1541-1569, 2012.

652 Luecken, D., Napelenok, S., Strum, M., Scheffe, R., and Phillips, S.: Sensitivity of ambient atmospheric
653 formaldehyde and ozone to precursor species and source types across the United States, Environ. Sci. Technol.,
654 52, 4668–4675, https://doi.org/10.1021/acs.est.7b05509, 2018.

655 Lui, K. H., Ho, S. S. H., Louie, P. K. K., Chan, C. S., Lee, S. C., Hu, D., Chan, P. W., Lee, J. C. W., and Ho,
656 K. F.: Seasonal behavior of carbonyls and source characterization of formaldehyde (HCHO) in ambient air,
657 Atmos. Environ., 152, 51-60, 10.1016/j.atmosenv.2016.12.004, 2017.

658 Mo, Z., Shao, M., Lu, S., Niu, H., Zhou, M., and Sun, J.: Characterization of non-methane hydrocarbons and
659 their sources in an industrialized coastal city, Yangtze River Delta, China, Sci Total Environ, 593-594, 641-
660 653, 10.1016/j.scitotenv.2017.03.123, 2017.

661 Na, K., Kim, Y. P., Moon, I., and Moon, K.-C.: Chemical composition of major VOC emission sources in the
662 Seoul atmosphere, Chemosphere, 55, 585-594, 10.1016/j.chemosphere.2004.01.010, 2004.

663 Norris, G., Duvall, R., Brown, S., Bai, S.: EPA positive matrix factorization PMF5.0 fundamentals and user
664 guide, 2014.

665 Nussbaumer, C. M., Crowley, J. N., Schuladen, J., Williams, J., Hafermann, S., Reiffs, A., Axinte, R., Harder,
666 H., Ernest, C., Novelli, A., Sala, K., Martinez, M., Mallik, C., Tomsche, L., Plass-Dülmer, C., Bohn, B.,
667 Lelieveld, J., and Fischer, H.: Measurement report: Photochemical production and loss rates of formaldehyde
668 and ozone across Europe, Atmos. Chem. Phys., 21, 18413-18432, 10.5194/acp-21-18413-2021, 2021.

669 Possanzini, M., Di Palo, V., & Cecinato, A.: Sources and photodecomposition of formaldehyde and
670 acetaldehyde in Rome ambient air. Atmos. Environ., 36(19), 3195–3201. https://doi.org/10.1016/S1352-
671 2310(02)00192-9, 2002.

672 Ren, X., Brune, W. H., Cantrell, C. A., Edwards, G. D., Shirley, T., Metcalf, A. R., and Lesher, R. L.: Hydroxyl
673 and peroxy radical chemistry in a rural area of Central Pennsylvania: Observations and model comparisons, J.
674 Atmos. Chem., 52, 231-257, 10.1007/s10874-005-3651-7, 2005.

675 Rollins, A. W., Browne, E. C., Min, K. E., Pusede, S. E., Wooldridge, P. J., Gentner, D. R., Goldstein, A. H.,
676 Liu, S., Day, D. A., Russell, L. M., and Cohen, R. C.: Evidence for NOx Control over Nighttime SOA
677 Formation, Science, 337, 1210–1212, 2012.

678 Sarkar, C., Sinha, V., Sinha, B., Panday, A. K., Rupakheti, M., and Lawrence, M. G.: Source apportionment
679 of NMVOCs in the Kathmandu Valley during the SusKat-ABC international field campaign using positive
680 matrix factorization, Atmos. Chem. Phys., 17, 8129-8156, 10.5194/acp-17-8129-2017, 2017.

681 Saunders, S. M., Jenkin, M. E., Derwent, R. G., and Pilling, M. J.: Protocol for the development of the Master

https://doi.org/10.5194/acp-2022-292
Preprint. Discussion started: 17 May 2022


Atmospheric Chemistry and Physics Discussions

682 Chemical Mechanism, MCM v3 (Part A): tropospheric degradation of nonaromatic volatile organic
683 compounds, Atmos. Chem. Phys., 3, 161–180, doi:10.5194/acp-3-161-2003, 2003.

684 Shen, H., Liu, Y., Zhao, M., Li, J., Zhang, Y., Yang, J., Jiang, Y., Chen, T., Chen, M., Huang, X., Li, C., Guo,
685 D., Sun, X., Xue, L., and Wang, W.: Significance of carbonyl compounds to photochemical ozone formation
686 in a coastal city (Shantou) in eastern China, Sci. Total Environ, 764, 144031, 10.1016/j.scitotenv.2020.144031,
687 2021.

688 Sindelarova, K., Markova, J., Simpson, D., Huszar, P., Karlicky, J., Darras, S., and Granier, C.: High-resolution
689 biogenic global emission inventory for the time period 2000–2019 for air quality modelling, Earth Syst. Sci.
690 Data, 14, 251-270, 10.5194/essd-14-251-2022, 2022.

691 Sinha, B., and Sinha, V.: Source apportionment of volatile organic compounds in the northwest Indo-Gangetic
692 Plain using a positive matrix factorization model, Atmos. Chem. Phys., 19, 15467-15482, 10.5194/acp-19-
693 15467-2019, 2019.

694 Tan, Z., Fuchs, H., Lu, K., Hofzumahaus, A., Bohn, B., Broch, S., Dong, H., Gomm, S., Häseler, R., He, L.,
695 Holland, F., Li, X., Liu, Y., Lu, S., Rohrer, F., Shao, M., Wang, B., Wang, M., Wu, Y., Zeng, L., Zhang, Y.,
696 Wahner, A., and Zhang, Y.: Radical chemistry at a rural site (Wangdu) in the North China Plain: observation
697 and model calculations of OH, HO_2 and RO_2 radicals, Atmos. Chem. Phys., 17, 663–690,
698 https://doi.org/10.5194/acp17-663-2017, 2017.

699 Villanueva, F., Lara, S., Amo-Salas, M., Cabañas, B., Martín, P., and Salgado, S.: Investigation of
700 formaldehyde and other carbonyls in a small urban atmosphere using passive samplers. A comprehensive data
701 analysis, Microchem. J., 167, 106270, 10.1016/j.microc.2021.106270, 2021.

702 Wang, C., Huang, X., Han, Y., Zhu, B., and He, L.: Sources and Potential Photochemical Roles of
703 Formaldehyde in an Urban Atmosphere in South China, J. Geophys. Res.-Atmos., 122, 11,934-911,947,
704 10.1002/2017jd027266, 2017.

705 Wittrock, F., Richter, A., Oetjen, H., Burrows, J. P., Kanakidou, M., Myriokefalitakis, S., Volkamer, R., Beirle,
706 S., Platt, U., and Wagner, T.: Simultaneous global observations of glyoxal and formaldehyde from space,
707 Geophys. Res. Lett., 33, L16804, https://doi.org/10.1029/2006GL026310, 2006.

708 Wolfe, G. M., Kaiser, J., Hanisco, T. F., Keutsch, F. N., de Gouw, J. A., Gilman, J. B., Graus, M., Hatch, C.
709 D., Holloway, J., Horowitz, L. W., Lee, B. H., Lerner, B. M., Lopez-Hilifiker, F., Mao, J., Marvin, M. R.,
710 Peischl, J., Pollack, I. B., Roberts, J. M., Ryerson, T. B., Thornton, J. A., Veres, P. R., and Warneke, C.:
711 Formaldehyde production from isoprene oxidation across NOx regimes, Atmos Chem Phys, 16, 2597-2610,
712 10.5194/acp-16-2597-2016, 2016.

713 World Health Organization (WHO): Guidelines for Air Quality. World Health Organization, Geneva,
714 Switzerland, 2000.

715 Wu, F., Sun, J., Yu, Y., Tang, G., and Wang, Y.: Variation Characteristics and Sources Analysis of Atmospheric
716 Volatile Organic Compounds in Changbai Mountain Station, Environ. Sci., 37, 3308-3314,
717 10.13227/j.hjkx.2016.09.008, 2016.

718 Wu, X., Xu, L., Hong, Y., Chen, J., Qiu, Y., Hu, B., Hong, Z., Zhang, Y., Liu, T., Chen, Y., Bian, Y., Zhao, G.,
719 Chen, J., and Li, M.: The air pollution governed by subtropical high in a coastal city in Southeast China:
720 Formation processes and influencing mechanisms, Sci Total Environ, 692, 1135-1145,
721 10.1016/j.scitotenv.2019.07.341, 2019.

722 Xue, L., Gu, R., Wang, T., Wang, X., Saunders, S., Blake, D., Louie, P. K. K., Luk, C. W. Y., Simpson, I., Xu,

https://doi.org/10.5194/acp-2022-292
Preprint. Discussion started: 17 May 2022

Z., Wang, Z., Gao, Y., Lee, S., Mellouki, A., and Wang, W.: Oxidative capacity and radical chemistry in the polluted atmosphere of Hong Kong and Pearl River Delta region: analysis of a severe photochemical smog episode, Atmos. Chem. Phys., 16, 9891–9903, 10.5194/acp-16-9891-2016, 2016.

Yang, X., Xue, L., Wang, T., Wang, X., Gao, J., Lee, S., Blake, D. R., Chai, F., and Wang, W.: Observations and Explicit Modeling of Summertime Carbonyl Formation in Beijing: Identification of Key Precursor Species and Their Impact on Atmospheric Oxidation Chemistry, J. Geophys. Res.-Atmos., 123, 1426-1440, 10.1002/2017jd027403, 2018.

Yang, X., Zhang, G., Sun, Y., Zhu, L., Wei, X., Li, Z., and Zhong, X.: Explicit modeling of background HCHO formation in southern China, Atmos. Res., 240, 104941, 10.1016/j.atmosres.2020.104941, 2020.

Yang Y, Shao M, Keßel S, Li Y, Lu K, Lu S, Williams J, Zhang Y, Zeng L, Nölscher AC et al: How the OH reactivity affects the ozone production efficiency: case studies in Beijing and Heshan, China. Atmos. Chem. Phys., 17(11), 7127-7142, 2017.

Yang Y, Shao M, Wang X, Nölscher AC, Kessel S, Guenther A, Williams J: Towards a quantitative understanding of total OH reactivity: A review. Atmos. Environ., 134, 47-161, 2016.

Zeng, P., Lyu, X., Guo, H., Cheng, H., Wang, Z., Liu, X., and Zhang, W.: Spatial variation of sources and photochemistry of formaldehyde in Wuhan, Central China, Atmos. Environ., 214, 116826, 10.1016/j.atmosenv.2019.116826, 2019.

Zhang, K., Duan, Y., Huo, J., Huang, L., Wang, Y., Fu, Q., Wang, Y., and Li, L.: Formation mechanism of HCHO pollution in the suburban Yangtze River Delta region, China: A box model study and policy implementations, Atmos. Environ., 267, 118755, 10.1016/j.atmosenv.2021.118755, 2021a.

Zhang, K., Huang, L., Li, Q., Huo, J., Duan, Y., Wang, Y., Yaluk, E., Wang, Y., Fu, Q., and Li, L.: Explicit modeling of isoprene chemical processing in polluted air masses in suburban areas of the Yangtze River Delta region: radical cycling and formation of ozone and formaldehyde, Atmos. Chem. Phys., 21, 5905-5917, 10.5194/acp-21-5905-2021, 2021b.

Zhang L , Brook J R , Vet R . A revised parameterization for gaseous dry deposition in air-quality models. Atmos. Chem. Phys., 3(2), 2067-2082, 2003.

Zhang, Y., Xue, L., Carter, W., Pei, C., and Wang, W.: Development of Ozone Reactivity Scales for Volatile Organic Compounds in a Chinese Megacity, Atmos. Chem. Phys., 10.5194/acp-2021-44, 2021.

Zhou, X., Huang, G., Civerolo, K., Roychowdhury, U., and Demerjian, K. L.: Summertime observations of HONO, HCHO, and O_3 at the summit of Whiteface Mountain, New York, J. Geophys. Res., 112, 1-13, 10.1029/2006jd007256, 2007.

Zhu, J., Wang, S., Wang, H., Jing, S., Lou, S., Saiz-Lopez, A., and Zhou, B.: Observationally constrained modeling of atmospheric oxidation capacity and photochemical reactivity in Shanghai, China, Atmos. Chem. Phys., 20, 1217-1232, 10.5194/acp-20-1217-2020, 2020.